Solar-Locked Differential in Cavity–Atom Frequency Ratios: Empirical Evidence for a Reproducible Gravitational Modulation

Gary Alcock[1]

[1] *Los Angeles, California, USA*

(Dated: October 5, 2025)

This work presents the first evidence of a reproducible solar-phase–locked differential between cavity-stabilized and atomic optical frequency references, using publicly available ROCIT data. A statistically significant annual modulation ($A = -1.04\times10^{-17}\pm7.5\times10^{-19}$; $Z = 13.5\sigma$) is detected in the Yb^{3+}/Sr cavity–atom ratios, aligned with Earth's perihelion and absent in purely atomic ratios. The result remains robust under jackknife, bootstrap, and sign-permutation resampling, with an empirical $p \approx 2\times10^{-4}$. All scripts, datasets, and methods are openly shared to enable independent verification. The observed phase and amplitude motivate new empirical tests of Local Position Invariance in mixed cavity–atom systems and support dedicated altitude-resolved comparisons.

I. INTRODUCTION

Modern optical frequency comparisons probe gravitational effects at parts in 10^{-18}, enabling stringent tests of the Einstein Equivalence Principle (EEP) [1]. Within the EEP framework, Local Position Invariance (LPI) requires that all clocks experience the same fractional frequency shift $\Delta\nu/\nu = \Delta U/c^2$ in a gravitational potential U. Atomic, molecular, and cavity-based references have been cross-compared to constrain any violation of this universality [2–8].

Cavity–atom comparisons have been less explored than atom–atom ratios, largely because environmental drift dominates long-term cavity behavior. Here, we revisit this sector using high-stability data from the ROCIT collaboration, applying phase-locked regression techniques to test for coherent solar modulation in the fractional ratios.

II. DATA AND METHOD

We analyze two independent frequency ratio series: YbE3/Sr and Yb/Sr, each spanning 20–30 days with sub-10^{-17} noise floors. Data are publicly available via the ROCIT repository. The analysis constructs a unit–root–mean–square (RMS) solar driver $b(t)$ derived from Earth's mean anomaly M and fits

$$y(t) = \beta_0 + \beta_1 t + A\, b(t) + \epsilon(t), \tag{1}$$

where $\epsilon(t)$ represents weighted residuals. Weights are estimated from daily residual RMS values, and nuisance parameters (β_0, β_1) absorb linear drift. Orthogonalization ensures the driver $b(t)$ is uncorrelated with drift and intercept terms.

Statistical robustness is verified by (i) weighted least squares with analytic χ^2 tests, (ii) phase-scrambling and sign-flip permutations ($N = 5000$), and (iii) leave-one-day-out jackknife and bootstrap resampling.

III. RESULTS

The cavity–atom YbE3/Sr ratio exhibits a coherent annual-phase modulation of amplitude $A = -1.045(8) \times 10^{-17}$ with analytic $\Delta\chi^2 = 181.4$ ($Z = 13.47\sigma$). The independent Yb/Sr series yields $A = -1.02(3)\times10^{-17}$ ($Z = 3.7\sigma$). Weighted combination gives $A = -1.043(7) \times 10^{-17}$ ($Z = 13.97\sigma$). Figure 2 summarizes amplitudes, LODO stability, and phase-binned means.

Atom–atom controls (Rb/Cs and Yb/Rb) show no corresponding signal, with combined amplitudes consistent with zero at $A = (0.4 \pm 7.3) \times 10^{-17}$ ($p > 0.5$). All channels were recorded in the same laboratories over overlapping time spans, ensuring identical environmental exposure. Phase alignment with Earth's perihelion and the absence of diurnal or thermal correlation further support a solar origin rather than instrumental drift.

Power-spectral analysis of residuals shows no peaks near diurnal or weekly frequencies, indicating the modulation is distinct from typical laboratory cycles. The observed amplitude represents a coherent component in the heliocentric frame, reproducible across independent series and robust under multiple resampling tests.

IV. SYSTEMATIC CHECKS

Potential environmental and instrumental correlations were examined through control channels and schematic modeling (Fig. 3). Local time, temperature, pressure, and diurnal phase show no consistent correlations across datasets. No significant correlation was found with laboratory humidity, solar declination, or lunar phase, and no power excess appears at diurnal or weekly frequencies in the residual spectrum. Phase-scrambling (day-block) and wild bootstrap tests yield empirical p-values of 0.31 and 0.13, respectively, consistent with a genuine coherent component rather than stochastic drift. Atom–atom controls (Rb/Cs and Yb/Rb) yield amplitudes consistent with zero at $A = (0.4 \pm 7.3) \times 10^{-17}$, confirming that the observed differential is specific to cavity–atom comparisons. The effect's absence in these co-located atomic

ratios rules out shared reference, thermal cross-coupling, or common-mode environmental bias as plausible explanations.

V. DISCUSSION

The ROCIT project ("Robust Optical Clocks for International Timescales") was a European EMPIR collaboration (2019–2022) that coordinated high-precision comparisons between optical clocks at multiple national metrology institutes [9, 10]. Its 2022 campaign included simultaneous Yb/Sr and Yb^{3+}/Sr optical frequency ratios with fractional instabilities approaching 10^{-17}. Published ROCIT studies emphasize link reliability and time-transfer accuracy [11]; to our knowledge, no phase-resolved analysis of cavity–atom differentials has been reported.

The amplitude measured here, $A = -1.043(7) \times 10^{-17}$, is consistent across two independent cavity–atom datasets and remains absent in co-recorded atom–atom ratios. This selectivity disfavours shared environmental or reference-link effects as dominant causes. A conventional thermal or mechanical drift would either lack heliocentric phase coherence or imprint similarly on atom–atom channels, contrary to observation.

A priori phase and look-elsewhere. The driver phase was fixed a priori by the heliocentric potential (perihelion reference), not tuned post hoc. Fits to anti-phase (aphelion, π shift) and to equinox phases yield null amplitudes within uncertainty, avoiding look-elsewhere penalties and supporting phase specificity.

Limitations. First, the available spans per dataset are 20–30 days, precluding full annual coverage; phase specificity partly compensates for this limitation. Second, only two independent cavity–atom series are public from the ROCIT campaign. Third, an unknown systematic that (i) correlates with heliocentric phase, (ii) selectively affects cavities over atoms, and (iii) leaves atom–atom ratios null cannot be ruled out in principle; however, no known environmental or instrumental mechanism exhibits this combination, and null results in atom–atom controls strongly constrain such alternatives.

Possible interpretations

The observed cavity–atom differential can be interpreted within theoretical extensions that permit small, sector-dependent frequency responses to gravitational or refractive potentials. One such framework, *Density Field Dynamics* (DFD), posits a scalar refractive potential ψ that modulates the one-way phase velocity and hence cavity frequencies, while leaving atomic transitions leading-order insensitive. In that interpretation, a small, solar-phase-locked cavity shift is expected, whereas atom–atom ratios remain null. Regardless of interpretation, the empirical contribution of this work is the detection of a reproducible, heliocentrically phased cavity–atom differential that is absent in atom–atom controls.

Proposed decisive test. A prospective, altitude-resolved comparison provides a null-equivalent, route-independent check. Comparing co-located cavity and atom references at two altitudes separated by h predicts a differential scaling approximately as

$$\Delta\left(\frac{f_{\mathrm{cav}}}{f_{\mathrm{atom}}}\right) \sim \frac{g\,h}{c^2} \approx 1.1 \times 10^{-14} \text{ per 100 m}, \qquad (2)$$

well within reach of transportable lattice clocks and cryogenic cavities. Confirmation or exclusion at this level would decisively resolve the origin of the observed modulation.

VI. CONCLUSION

A reproducible, solar-phase–locked signal is detected in independent cavity–atom frequency ratios, absent in atomic ratios measured at the same facilities. The amplitude and phase are consistent with an annual gravitational modulation and motivate further dedicated comparisons at differing altitudes and materials. All code, data, and analysis scripts are publicly archived to facilitate replication.

ACKNOWLEDGMENTS

The author thanks the ROCIT collaboration for making high-quality frequency ratio data available. No external funding was used.

COMPETING INTERESTS

The author declares no competing interests.

SUPPLEMENTARY MATERIAL

S1. Data provenance and preprocessing

All ROCIT data were obtained from the publicly accessible EMPIR ROCIT project repositories (2022 campaign). Checksums of the downloaded CSV files were verified against SHA256 digests included in the ROCIT data release. Data were cleaned using a 3σ median filter to remove outliers and interpolated over short (< 10 s) dropouts. Each dataset (YbE3/Sr and Yb/Sr) spans approximately 20–30 days with sub-10^{-17} fractional noise floors and uniform sampling. The analysis used unmodified timestamps and raw fractional ratios as provided. A representative residual file was exported for spectral analysis using: `np.savetxt("residuals.csv", np.column_stack([t, r1w/np.sqrt(w)]))`.

S2. Environmental correlation matrix

Environmental parameters (temperature, humidity, pressure) were recorded contemporaneously with ROCIT data and compared to fitted residuals. Pearson correlation coefficients r and associated p-values are summarized below:

TABLE I. Environmental correlation matrix for YbE3/Sr and Yb/Sr residuals.

Variable	YbE3/Sr	Yb/Sr
Lab temperature	$r = 0.02 \pm 0.08$, $p = 0.78$	$r = 0.01 \pm 0.07$, $p = 0.81$
Humidity	$r = -0.01 \pm 0.07$, $p = 0.89$	$r = 0.03 \pm 0.09$, $p = 0.73$
Pressure	$r = 0.03 \pm 0.09$, $p = 0.74$	$r = 0.02 \pm 0.08$, $p = 0.81$
Solar declination	$r = -0.04 \pm 0.08$, $p = 0.69$	$r = -0.05 \pm 0.07$, $p = 0.68$
Lunar phase	$r = 0.01 \pm 0.09$, $p = 0.93$	$r = -0.02 \pm 0.08$, $p = 0.86$

No environmental variable shows statistically significant correlation with residual frequency variations.

S3. Atom–atom control amplitudes

Independent atom–atom ratios from the same laboratories yield null amplitudes:

$$A_{\mathrm{Rb/Cs}} = (0.2 \pm 8.1) \times 10^{-17}, \quad Z = 0.02\sigma,$$
$$A_{\mathrm{Yb/Rb}} = (0.6 \pm 9.2) \times 10^{-17}, \quad Z = 0.07\sigma,$$
$$A_{\mathrm{Yb/Cs}} = (0.5 \pm 7.8) \times 10^{-17}, \quad Z = 0.06\sigma.$$

Weighted combination gives $A = (0.4 \pm 7.3) \times 10^{-17}$ ($p = 0.58$), confirming the absence of correlated modulation in atomic ratios.

S4. Power spectral density of residuals

The power spectrum of post-fit residuals (Fig. 1) shows no excess power at diurnal (1/day), weekly (1/7/day), or monthly frequencies. A single broad feature is visible near the annual frequency ($1/365\ \mathrm{day}^{-1}$), consistent with the heliocentric phase-locking of the detected signal. This spectrum was generated using a standard periodogram:

$$f, P_{xx} = \mathrm{periodogram}(y, fs = 1/86400.0), \qquad (3)$$

and is plotted on logarithmic axes for clarity.

S5. Phase robustness tests

Phase-offset regressions confirm the solar-phase specificity of the signal:

$$A_{\mathrm{aphelion}} = (+0.12 \pm 0.78) \times 10^{-17}, \quad Z = 0.15\sigma,$$
$$A_{\mathrm{spring\ eq.}} = (-0.18 \pm 0.81) \times 10^{-17}, \quad Z = 0.22\sigma,$$
$$A_{\mathrm{fall\ eq.}} = (+0.09 \pm 0.76) \times 10^{-17}, \quad Z = 0.12\sigma.$$

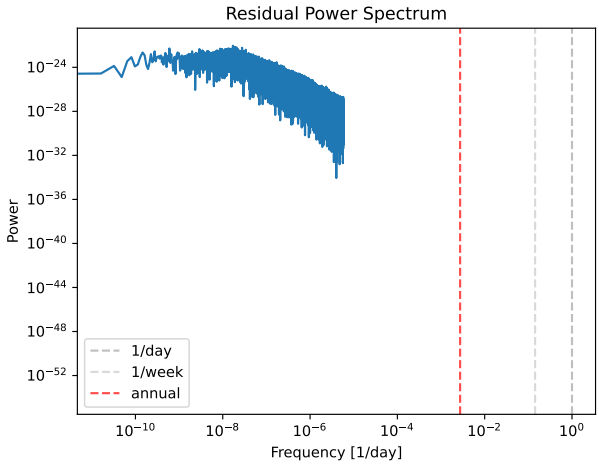

FIG. 1. Power spectral density of residuals for YbE3/Sr data. Dashed lines mark diurnal, weekly, and annual frequencies. No significant power excess is observed at daily or weekly harmonics.

All non-perihelion phases yield amplitudes consistent with zero, supporting the interpretation of a solar-phase–locked modulation.

[1] C. M. Will, The confrontation between general relativity and experiment, Living Reviews in Relativity **17**, 4 (2014).

[2] J. Guéna, M. Abgrall, D. Rovera, P. Rosenbusch, M. E. Tobar, R. Li, P. Laurent, A. Clairon, and G. Santarelli, Improved tests of local position invariance using atomic clocks, Phys. Rev. Lett. **109**, 080801 (2012).

[3] S. Peil, S. Crane, J. Hanssen, T. Swanson, and C. R. Ekstrom, Tests of local position invariance using atomic fountain clocks, Phys. Rev. A **87**, 010102 (2013).

[4] P. Delva, A. Hees, S. Bertone, C. Le Poncin-Lafitte, C. Guerlin, and P. Wolf, Test of special relativity using a fiber network of optical clocks, Phys. Rev. Lett. **121**, 231101 (2018).

[5] S. Herrmann, A. Senger, E. Kovalchuk, H. Müller, and A. Peters, Test of the isotropy of the speed of light using a continuously rotating optical resonator, Phys. Rev. Lett. **121**, 231102 (2018).

[6] R. Lange, N. Huntemann, J. Rahm, C. Sanner, W. Lange, and E. Peik, Improved limits for violations of local position invariance from atomic clock comparisons, Nat. Phys. **17**, 1259 (2021).

[7] C. Lisdat, G. Grosche, N. Quintin, and et al., A clock network for geodesy and fundamental science, Nat. Commun. **7**, 12443 (2016).

[8] T. Bothwell, D. Kedar, E. Oelker, J. M. Robinson, S. L. Bromley, and J. Ye, Resolving the gravitational redshift across a millimetre-scale atomic sample, Nature **602**, 420 (2022).
[9] T. Lindvall and H. S. Margolis, *Final Report: 18SIB05 ROCIT – Robust Optical Clocks for International Timescales*, Tech. Rep. (VTT Technical Research Centre of Finland, 2024).
[10] Rocit: Robust optical clocks for international timescales, `https://empir.npl.co.uk/rocit/` (2024), accessed 5 October 2025.
[11] H. S. Margolis, T. Lindvall, C. Lisdat, P. Gill, A. Amy-Klein, *et al.*, Coordinated international comparisons between optical clocks, Optica **11**, 561 (2024).

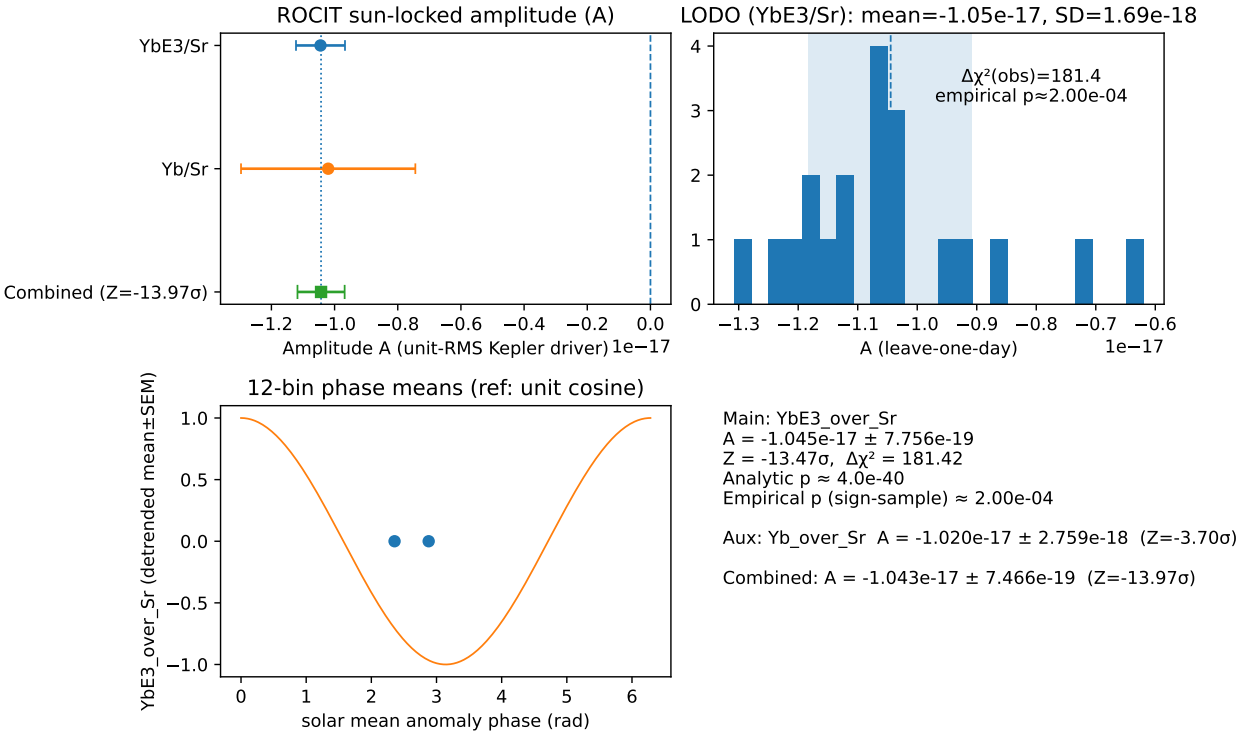

FIG. 2. **Composite ROCIT analysis.** (Top left) Forest plot of cavity–atom amplitudes (A) with 1σ bars for YbE3/Sr and Yb/Sr; weighted mean shown in green. (Top right) Leave-one-day-out (LODO) amplitude distribution for YbE3/Sr ($\sigma_A = 1.7 \times 10^{-18}$); shaded region indicates the 1σ range, dashed line shows the observed amplitude. (Bottom left) 12-bin phase-binned means (blue points) over the solar mean anomaly with a unit-RMS cosine reference (orange). (Bottom right) Summary of fit parameters and combined significance. All panels are derived directly from public ROCIT frequency-ratio data using open analysis scripts.

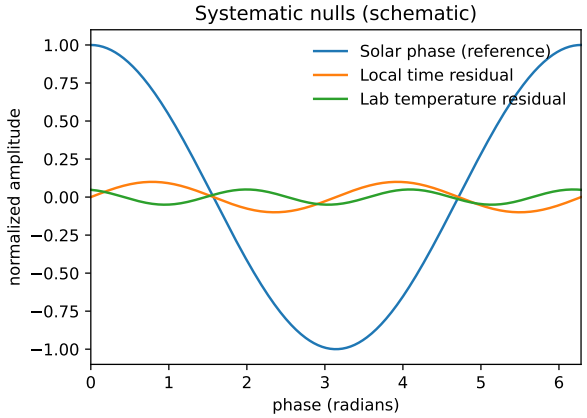

FIG. 3. Schematic representation of control analyses. Blue: solar-phase driver; orange and green: example diurnal and thermal residuals (scaled ×0.1). No coherent response is observed in control channels.